



# Dynamic Characterization and Vibration Analysis of a Four-Story Mass Timber Building

Ignace Mugabo<sup>1,2</sup>, Andre R. Barbosa<sup>1\*</sup> and Mariapaola Riggio<sup>2</sup>

<sup>1</sup> School of Civil and Construction Engineering, Oregon State University, Corvallis, OR, United States, <sup>2</sup> Department of Wood Science and Engineering, Oregon State University, Corvallis, OR, United States

## OPEN ACCESS

### Edited by:

Costas Papadimitriou,  
University of Thessaly, Greece

### Reviewed by:

Ertugrul Taciroglu,  
University of California, Los Angeles,  
United States  
Agathoklis Giaralis,  
City University of London,  
United Kingdom

### \*Correspondence:

Andre R. Barbosa  
Andre.Barbosa@oregonstate.edu

### Specialty section:

This article was submitted to  
Structural Sensing,  
a section of the journal  
Frontiers in Built Environment

**Received:** 19 January 2019

**Accepted:** 18 June 2019

**Published:** 04 July 2019

### Citation:

Mugabo I, Barbosa AR and Riggio M  
(2019) Dynamic Characterization and  
Vibration Analysis of a Four-Story  
Mass Timber Building.  
Front. Built Environ. 5:86.  
doi: 10.3389/fbuil.2019.00086

Mass timber construction has been gaining momentum in multi-story residential and commercial construction sectors in North America. As taller mass timber buildings are being planned and constructed, *in-situ* dynamic tests of this type of construction can be performed to further validate their design and use. As part of this larger effort, an *in-situ* dynamic characterization testing campaign based on ambient vibration measurements was conducted on a recently constructed four-story mass timber building located in Portland, Oregon. The building features cross-laminated timber (CLT) floors, a glued laminated timber (GLT) framing gravity system, and light-frame shear walls and steel HSS hold-downs that compose the lateral resisting system of the building. Ambient vibration acceleration testing data were collected using 18 accelerometers that were wired to a portable data acquisition system in two experimental setups. Approximately 2 h of bi-directional horizontal acceleration data were recorded. In this paper, two operational modal analysis methods are used for estimating the modal parameters (frequency, damping, and mode shapes) based on the data collected. In addition, a multi-stage linear Finite Element (FE) model updating procedure is presented for this building type and the FE estimates of frequencies and mode shapes are compared to estimates from the collected data. The calibrated FE model provides confidence to the operational modal results and presents a comprehensive modal characterization of the building. At ambient levels of excitation, the developed FE model suggests that stiffness of the non-structural elements, such as the exterior wall cladding, and glazing affects the modal response of the building considerably. Lessons learnt on this unique and first of a kind four-story structure constructed in the United States and implications for taller mass timber buildings are summarized and provide valuable insight for the design and assessment for this building type under future dynamic excitation events.

**Keywords:** cross-laminated timber, enhanced frequency domain decomposition, finite element modeling, light-framed shear walls, mass timber building, operational modal analysis, stochastic subspace identification

## INTRODUCTION

The last decade has been marked with a rise in interest and use of mass timber construction in North America (Pei et al., 2016). This rise is driven by a range of innovative wooden structural products such as cross-laminated timber (CLT) (Gagnon and Popovski, 2011), mass plywood panel (MPP) (Freres, 2018), and more traditional wooden products such as glued laminated timber

(GLT). These products are typically used in structural systems in conjunction with other wooden and non-wooden structural members. One example of such combination is the use of CLT walls with light-frame shear walls (Nguyen et al., 2018). In the past, light-frame shear wall systems have extensively been used in the residential industry, typically for one to two story homes, but also in construction of multi-story timber structures up to five stories high. With the use of mass timber structural products along with light-frame shear wall systems, a new opportunity in expanding the use of light-frame construction to a larger variety of occupancy types and to higher building heights has presented itself. This new opportunity warrants the need to improve the understanding of the performance of lateral dynamic behavior of this combined mass timber/light-frame structural system, especially of actual constructed facilities.

The dynamic behavior of a structure can be evaluated given two types of external excitations: (1) free vibration, with the structure subjected to initial input(s) only; (2) forced vibration, with the structure subjected to continuous input(s); and (3) ambient vibration, with the structure responding to ambient loads such as wind, traffic and/or human activities. Ambient vibration testing offers means to evaluate dynamic parameters without causing excitation induced discomfort to its occupants and eliminating the potential of causing excitation induced damage to the structure. When using ambient vibration testing, output only methods known as operational modal analysis (OMA) are typically used to identify structural system natural frequencies, damping ratios, and mode shapes from vibration testing using output only methods. Several OMA have already been developed over the past decades. Among the widely used methods are the Enhanced Frequency Domain Decomposition (EFDD) (Brincker et al., 2001) and the Stochastic Subspace Identification (SSI) (Brincker and Andersen, 2006). Damping ratio estimation from ambient vibrations testing using the above mentioned OMA methods have shown considerable uncertainty (Magalhães et al., 2010; Moaveni et al., 2014). Magalhães et al. (2010) simulated the effects of adding non-proportional damping and closely spaced natural frequencies to the damping estimation by the EFDD and SSI methods, and results indicated that the SSI method displayed more accurate results than the EFDD method in evaluating the damping ratios of highly complex and non-proportionally damped simulated data. This study also evaluated the variability in damping ratios of three ambient vibrations tested large civil engineering structures using the SSI method. Large variability in damping ratios were observed with as much as 52% standard deviation relative to the mean damping ratio. Similar uncertainty was observed in the Moaveni et al. (2014) study. In an effort to draw comprehensive conclusions on modal damping ratios, Satake et al. (2003) compiled natural periods and damping data of 284 structures of height ranging mostly between 50 and 150 m. High correlations were observed between: (1) height of buildings and fundamental translational periods, (2) fundamental translational and torsional periods, and (3) fundamental periods and higher modes periods. Results in Satake et al. suggested that natural periods could be well-approximated as function of height. In general, reinforced concrete buildings had damping ratios above 2%, while steel-framed buildings had damping ratios below 2%. It was also noted that the first mode

damping ratios were inversely proportional to the height of the building. Office buildings, which tend to have fewer non-structural walls compared to apartment and hotel buildings, exhibited slightly lower first mode damping ratios than the apartment and hotel buildings.

The variations in modal parameters due to environmental loads (temperature, rain, wind), seismic ground shaking of varying intensity, and seismic retrofits have extensively studied in the past. Clinton et al. (2006) reported on the observed changes in natural frequencies of two buildings located at the California Institute of Technology. Over a span of 36 years, one of the buildings, the Millikan Library, experienced a decrease of 22 and 12% in the East-West and the North-South fundamental frequencies, respectively. The permanent reductions in frequencies were attributed to several moderate strong motions that the building experienced over the 36-year life span. Other factors such as heavy rain and strong winds also produced temporary changes in natural frequencies. Results indicated that natural frequencies increased up to 3% following heavy rain events. In another study conducted by Nayeri et al. (2008), ambient vibrations measurements on a 15-story steel frame structure were collected over a 50-day period. Changes in natural frequencies were mostly small with coefficients of variation (CVs) in the order of 1 to 2%, while damping ratios varied in the 20 to 70% range for CVs. Diurnal natural frequency variations ranging from 1 to 4% were observed and resulting from changes in temperature during the day. During and following the 1989 Loma Prieta earthquake, Çelebi et al. (1993) collected strong and ambient motions measurements on five San Francisco bay area buildings that exhibited no visible damage following the Loma Prieta earthquake. For each of the five buildings, the fundamental frequencies obtained during the strong motion responses were lower than those obtained during ambient vibration testing. The ratios of ambient to strong motion (ambient/strong motion) fundamental frequency ranged from 1.47 to 1.14. The difference in fundamental frequencies could be the result of several factors such as: (1) soil structure interaction, (2) non-linear structural behavior, (3) slip of steel connections, and (4) interactions between structural and non-structural elements. Michel et al. (2009) compared weak earthquake to ambient vibrations of a 13-story permanently monitored reinforced concrete building in Grenoble, France. Decreases of up to 3% in natural frequencies were observed using ground motions measurements compared to ambient vibrations. With respect to the effect of seismic retrofits, Ivanović et al. (2000) described changes in natural frequencies of a severely damaged seven-story reinforced concrete building following the 1994 Northridge earthquake and its aftershocks. Ambient vibration measurements following (1) the main event and (2) one of main aftershocks indicated that the natural frequencies of the building increased up to 10% during the second data collection, most likely due to the additional wooden braces added near structurally damaged areas. Soyoz et al. (2013) evaluated the effects of retrofitting of a non-ductile reinforced concrete building. The various steps of the retrofitting effort included (1) the removal of infill masonry walls, (2) the addition of column jackets, and (3) the addition of structural walls. The removal of infill masonry walls decreased the fundamental frequency

by 11%, and the subsequent retrofit increased the fundamental frequency by 96% in relation to the fundamental frequency after infills removal.

Several studies have evaluated the ambient dynamic behavior of light-frame shear wall buildings (Ellis and Bougard, 2001; Camelo et al., 2002; Steiger et al., 2016; Hafeez et al., 2018). Ellis and Bougard (2001) performed dynamic testing and evaluated the stiffness of a six-story light-frame timber building during different phases of construction. In this study, the fundamental frequencies were measured, and lateral stiffness was evaluated throughout several stages of construction. As the construction of the building evolved, the fundamental frequencies of the building increased as non-structural components such as staircases, interior plasters, and brickwork were added. The effects of non-structural components on the behavior of structures under ambient vibrations have been observed by several studies independently of the lateral resisting system used (Clinton et al., 2006; Li et al., 2011; Asgarian and McClure, 2012; Devin and Fanning, 2012; Assi et al., 2016). Li et al. (2011) developed linear elastic finite element models of four tall buildings with some of them featuring non-structural components such as an aluminum façade and infill walls. As much as 60% stiffness increase from the non-structural components were observed. Devin and Fanning (2012) conducted ambient vibration testing on a four-story reinforced concrete frame structure with a lateral force resisting system consisting of a set of reinforced concrete cores. A linear elastic FE model of the structural system produced a natural frequency 24% lower compared to the ambient vibrations estimated values. This difference was attributed to the stiffness contribution of non-structural components. The differences in fundamental frequencies of light-frame shear wall structures tested under different levels of excitation have also been acknowledged by other studies (Kharrazi and Ventura, 2006; Hafeez et al., 2018). Notably, Kharrazi and Ventura (2006) suggested a simple equation relating the fundamental frequencies of light-frame low-rise structures obtained from ambient vibration to the ones obtained from forced vibrations dynamic characterization testing. Hafeez et al. (2018) evaluated fundamental periods and modal damping of 47 wood-frame buildings under ambient vibrations. The authors provided a fundamental period relationship based on the Rayleigh quotient (Chopra, 2012) and extended an equation developed in Kharrazi and Ventura (2006) for estimating fundamental frequencies of light-frame shear wall structures.

Extensive research has focused on modeling of wooden structural systems (Tarabia and Itani, 1997; Folz and Filiatrault, 2004a,b; Collins et al., 2005a,b). Noteworthy examples of interest to this paper are the Folz and Filiatrault (2004a,b), in which a numerical modeling approach for predicting the dynamic response of light-frame shear wall building systems was developed and validated. This modeling approach considers rigid horizontal diaphragms and non-linear lateral load resisting shear wall models, which correspond to shear spring elements connecting adjacent horizontal diaphragms or horizontal diaphragms to the foundation. The modeling approach was validated in Folz and Filiatrault (2004b). For this validation effort, two construction phases were chosen as comparison points: first, after the two-story structure was

sheathed with the OSB material, and second, after the interior gypsum wallboards and the exterior stucco were added to the structure. Results from the model prediction showed to be in good agreement with the test results, with maximum relative displacement values averaging 10% difference from the values obtained from the experimental campaign. Similarly to the studies described in the previous paragraph, the results from the testing and modeling also indicated that the natural frequency of the building changed from 3.28 to 6.95 Hz after the addition of gypsum wallboards and stucco increased.

The main objective of this paper is to provide a benchmark dataset on the dynamic characterization of an as-built hybrid mass timber construction of the first building constructed in the United States using US manufactured cross-laminated timber (CLT). The building, known as “Albina Yard,” is an example of a hybrid structure, exhibiting a mass timber gravity system, while its lateral force resisting system consists of light-frame shear walls. While extensive research has gone into characterizing the structural properties of mass timber members and sub-systems, few research studies have analyzed the dynamic behavior of buildings encompassing mass timber structural products, and specifically CLT (Reynolds et al., 2014, 2015, 2016; Hu et al., 2016). The limited number of currently built mass timber buildings, especially in North America, makes this endeavor more challenging, while it provides motivation for characterizing the as-built modal properties of this type of structures. This study contributes to this gap in knowledge and also improves the general understanding of the impact of drift sensitive non-structural components (NSCs) on natural frequencies. In this study, output-only modal analysis methods are used to determine the modal parameters (natural frequencies, mode shapes and damping ratios) of the Albina Yard from an *in-situ* ambient vibrations testing campaign conducted on the building shortly after its completion, in January of 2017. Ambient vibration testing was performed using 18 accelerometers in two experimental setups and a portable data acquisition system that recorded approximately 2 h of horizontal acceleration data. Two OMA methods were used for estimating the modal parameters. A finite element (FE) model that includes the structural and NSCs of the building is created for correlation with the results obtained in the OMA study. Based on the FE model, a parametric study that includes both structural and NSC parameters is conducted to inform the roles that structural and NSCs contribute in the dynamic behavior of the tested structure under ambient vibration. Finally, results from the output-only test and the model are compared to the approximate fundamental period code equations, commonly used by practicing engineers in the United States (American Society of Civil Engineers, 2017).

## STRUCTURAL DYNAMIC TESTING AND CHARACTERIZATION METHOD

### Building Description

The “Albina Yard” is a four-story mass timber building located in Northeast Portland, Oregon (**Figure 1**) whose construction was completed in 2017. The building has a general rectangular shape with open floor plans, two staircases near its South face

and an elevator shaft approximately near its geometric center in plan, as shown in **Figure 2**. For reference, **Figure 3** shows an elevation section of the building in the East-West direction through the middle of the building. The building has a footprint of approximately 26 m long (27.20 m to 25.45 m on depending story level) by 13.94 m with a total height of approximately 15.39 m above the grade level. The first story is dedicated to retail space, while upper stories are designed to be used as office space. The building envelope is comprised mainly of window glazing on the East and West façades and metal cladding walls on the North and South faces, with some small window and exterior door openings on the South façade.

The gravity load bearing system is composed of Douglas-fir (*Pseudotsuga menziesii*) glued laminated timber (GLT) columns and beams that support Douglas-fir (*Pseudotsuga menziesii*) three-ply cross-laminated timber (CLT) floors. The GLT column used are have two cross-sections:  $222 \times 229$  mm (GL  $8 \frac{3}{4}'' \times 9''$ ), and  $222 \times 305$  mm (GL  $8 \frac{3}{4}'' \times 12''$ ). The first column cross-section is used around the perimeter of the building, while the second one is used at interior load bearing locations. The primary GLT beams are distributed in plan following the gridlines shown in **Figure 2** and include two cross-section types:  $171 \times 457$  mm (GL  $6 \frac{3}{4}'' \times 18''$ ), and  $171 \times 610$  mm (GL  $6 \frac{3}{4}'' \times 24''$ ). The first type corresponds to the exterior beams spanning in the East-West direction and the North-South direction, while the second type is used as the primary interior beams running in the East-West direction. The spans for the beams are generally 6.10 m in the East-West direction with exception of one bay of the second floor level that is 2.78 m. In the North-South direction, the spans are 5.60 m and 7.43 m. In **Figure 2**, the gridlines for some secondary GLT girders spanning in the North-South direction are omitted from the figure for clarity of the figure. These omitted girders are located halfway between the gridlines shown in the North-South direction. Therefore, the typical spacing of beam axes for beams running in the North-South direction is 3.05 m, which serve as the primary span direction and span size of the CLT floors. Three-ply CLT floor panels, with approximate thickness of 104 mm (4.1"), are specified as ANSI PRG 320 Grade V2 (American National Standards Institute/APA—The Engineered Wood Association, 2018). The CLT floors are topped off with a 25.4 mm layer of non-structural lightweight concrete (Gyp-Crete).

The lateral load resisting system consists of double-sheathed plywood shear walls and a diaphragm provided by the CLT floors. The shear walls feature two types of hold-downs: (1) a hollow structural sections HSS  $127 \times 127$  mm  $\times$  6.4 mm (HSS  $5'' \times 5'' \times \frac{1}{4}''$ ) at the first and second level stories, and (2)  $150 \times 150$  mm ( $6'' \times 6''$  nominal size) solid sawn lumber posts on the third and fourth level stories. The sheathed plywood shear walls are located in the middle of the building and to South face of the building, close to the elevator shaft and the staircases.

## Testing Description: Instrumentation, Setup, and Procedures

This testing campaign was executed shortly after commissioning. Thus, the testing was carried out on a weekend day to

avoid interference with occupants' activities and minimize the input from human induced vibrations. The building was tested assuming ambient conditions (road traffic, wind, etc.). For this ambient vibration testing campaign, 16 uniaxial accelerometers and one (1) tri-axial accelerometer were used. The uniaxial accelerometers were PCB model 393B04 and the tri-axial accelerometer was a PCB model W356A12. **Figure 4** shows the two types of accelerometers and the data acquisition system used during the testing campaign. Further details on the accelerometer specifications are presented (Mugabo et al., 2019).

The accelerometers were distributed across the building and were attached to the underside of the CLT floors using glued metal brackets. The channels and the positive direction of the accelerations measured are indicated by the labels 1 to 18, shown in **Figure 2**. The channels 1 to 12 and 15 to 18 were connected to PCB 393B04 accelerometers while channels 13 and 14 are the X and Y components of the PCB W356A12 accelerometer used. **Figure 3** shows the vertical locations of the accelerometers throughout the building; however, it does not correctly represent the N-S direction locations (in/out-of-plane position) of the accelerometers.

Due to the time constraints and limited number of accelerometers used in this *in-situ* testing, the test was phased into two setups. The first phase, Setup-1, included six (6) accelerometers attached on the underside of the roof, as well as in the fourth- and third-floor levels. The second phase, Setup-2, included six (6) accelerometers on the underside of the roof and third floor level, two (2) accelerometers on the underside the fourth-floor level, and four (4) on the underside of the second-floor level. It is worth noting that the northwestern corner of the second-floor level was not instrumented because it was not accessible during the testing period. For each setup, the data were collected for approximately 1 h, with a sampling frequency of 2,048 Hz. Once ambient vibration data were collected, the PCB W356A12 accelerometer channels were deemed not sensitive enough for the application at hand.

## Data Post-processing and Analysis: Procedures and Methods

Data were analyzed using operational model analysis (OMA) techniques. The two OMA methods used in the estimation of the modal features are EFDD and SSI, following a similar approach used by Magalhães et al. (2007) and Moaveni et al. (2014), which are available in the software used (ARTEMIS Modal, 2017). More detailed explanations of the methods can be found in Brincker et al. (2001) for the EFDD and Brincker and Andersen (2006) for the SSI methods, respectively.

Before applying the two methods, however, the collected data were post-processed using power spectral densities (PSDs), taken on 1-min windows using the pwelch function from MATLAB's signal processing toolbox (MathWorks, 2018) to identify high noise signals or malfunctioning accelerometers, and eliminate corrupted data from the analysis. For the data analysis using the EFDD and SSI methods, a set of post-processing schemes were defined to focus on different sections of the frequency spectrum of interest. The processing schemes used



**FIGURE 1** | Photo of the Albina Yard building taken from the northeast corner.



**FIGURE 2** | Floor level plans showing the locations of accelerometers marked 1–18. Accelerometers 1–8 and 13–18, shown in red circles are the reference accelerometers. Roving accelerometers 9–12 are shown in yellow squares for setup 1 and black triangles for setup 2. The dimensions are presented in meters. (A) Second floor level, (B) Third floor level, (C) Fourth floor level, (D) Roof level.

are listed in **Table 1**. An upper limit of 20.48 Hz was considered adequate for capturing the first few natural frequencies of interest and various Butterworth filters windows were used to

focus on different sections of the spectrum of interest. The decimation frequencies of 10.24 and 5.12 Hz were used to focus on the lower natural frequencies. The processing steps

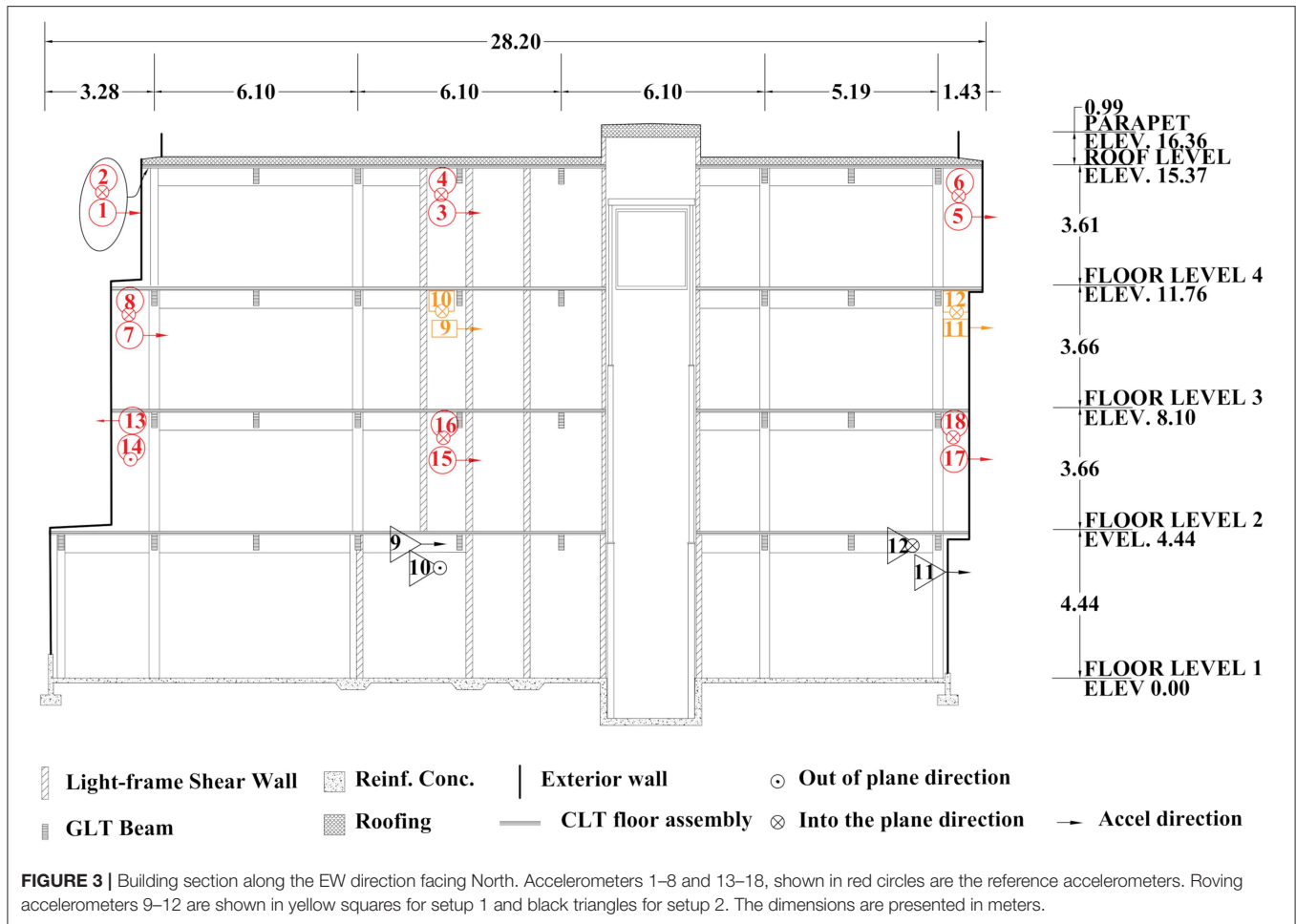


**FIGURE 3 |** Building section along the EW direction facing North. Accelerometers 1–8 and 13–18, shown in red circles are the reference accelerometers. Roving accelerometers 9–12 are shown in yellow squares for setup 1 and black triangles for setup 2. The dimensions are presented in meters.

**TABLE 1 |** Description of processing schemes.

Process	Analysis method	Decimation frequency (Hz)	Butterworth filter
1	EFDD	10.24	High-pass (0.5 Hz, $n = 3$ )
2	SSI	10.24	High-pass (0.5 Hz, $n = 3$ )
3*	EFDD	20.48	Band-pass(8–18 Hz, $n = 6$ )
4*	SSI	20.48	Band-pass(8–18 Hz, $n = 6$ )
5	EFDD	5.12	High-pass (0.5 Hz, $n = 6$ )
6	SSI	5.12	High-pass (0.5 Hz, $n = 6$ )
7*	EFDD	20.48	High-pass (0.5 Hz, $n = 3$ )
8*	SSI	20.48	High-pass (0.5 Hz, $n = 3$ )
9*	EFDD	20.48	High-pass (6.5 Hz, $n = 3$ )
10*	SSI	20.48	High-pass (6.5 Hz, $n = 3$ )

\*Harmonic peak reduction was used.

were performed on the combined sets of data and on each of the two separate sets of data (Setup-1 only and Setup-2 only). As a result, 30 different data analysis processing were performed. It is worth noting that harmonic peaks were observed in the frequency range of 12 Hz to the decimation frequency 20.48 Hz. To extract modal features in this frequency range,

a harmonic peak reduction algorithm integrated in ARTeMIS and based on an SSI process orthogonal projection was used (Gres et al., 2019).

### Structural Modeling

A SAP2000 (CSI, 2017) linear elastic finite element (FE) model was developed to correlate to the obtained OMA results. The model was developed to benchmark the experimental results and define a modeling strategy that can be applied to mass timber buildings with light-frame shear walls dynamically tested under ambient vibrations. To validate the identified natural frequencies at ambient level of excitation, a detailed model of the structure comprising of structural and non-structural members was required. The need for such a detailed model is due to the notion that, at ambient levels, the non-structural members contribute significantly to the lateral stiffness of the structure. To avoid difficulties that can arise from starting with a refined model, it was necessary to start with a simplified structural model and subsequently add non-structural components that are assumed to contribute to the lateral stiffness of the building. This multi-stage modeling approach is graphically illustrated in Figure 5. The first phase, phase 1, included the gravity loads supporting system and the light-frame shear walls. In

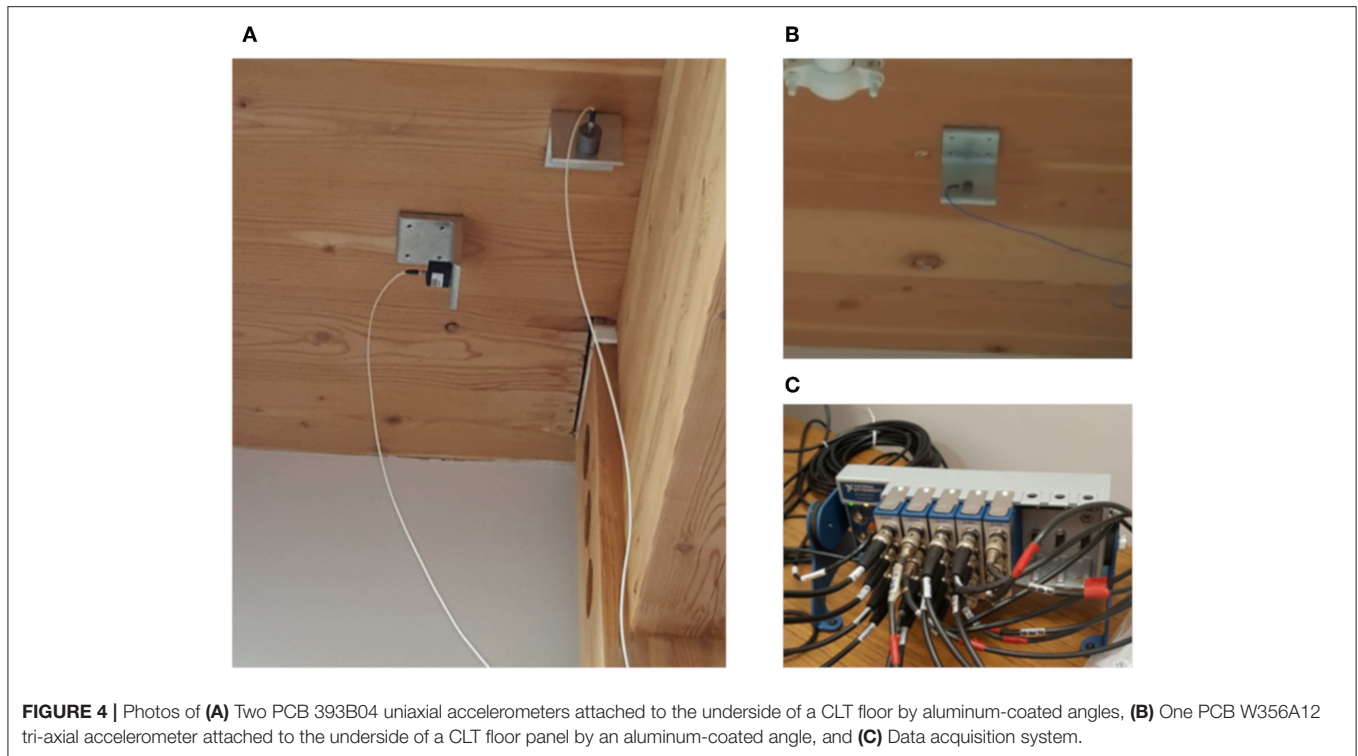


**FIGURE 4** | Photos of (A) Two PCB 393B04 uniaxial accelerometers attached to the underside of a CLT floor by aluminum-coated angles, (B) One PCB W356A12 tri-axial accelerometer attached to the underside of a CLT floor panel by an aluminum-coated angle, and (C) Data acquisition system.

phase 2 the non-structural wall components were added to the FE model, namely gypsum wallboards (gwb) layers. Following the addition of the components in phase 2, phase 3 included the exterior metal façade walls and window glazing. In phase 4 the staircase members were added to the FE model. Phase 1 through phase 4 included all the structural and non-structural building components that were considered to have effects on the lateral stiffness of the building at ambient levels. A correlation phase, phase 5, was added to adjust the model results to identified modal parameters.

The gravity loads resisting system, included in phase 1 of the model, consisted of GLT beams and columns, and the CLT floors. First, the GLT beams and columns were modeled as isotropic materials with an elastic modulus of 12,410 MPa as specified in the National Design Specification (NDS) Supplement manual (American Wood Council, 2015). It worth noting that NDS provides design values presenting lower bound values, and not necessarily indicate the expected values (median). The column base joints were modeled as fixed restraints to replicate the fixity behavior of column bases at ambient levels of loading. CLT floors were modeled as isotropic thin shell diaphragms with their nominal thickness and assigned a modulus of elasticity of 12,410 MPa (1,800 ksi). This nominal value in fact corresponds to assuming the CLT diaphragm in this case study is essentially rigid. **Table 2** provides a summary of the stiffness properties of all structural components used in the finite element modeling scheme.

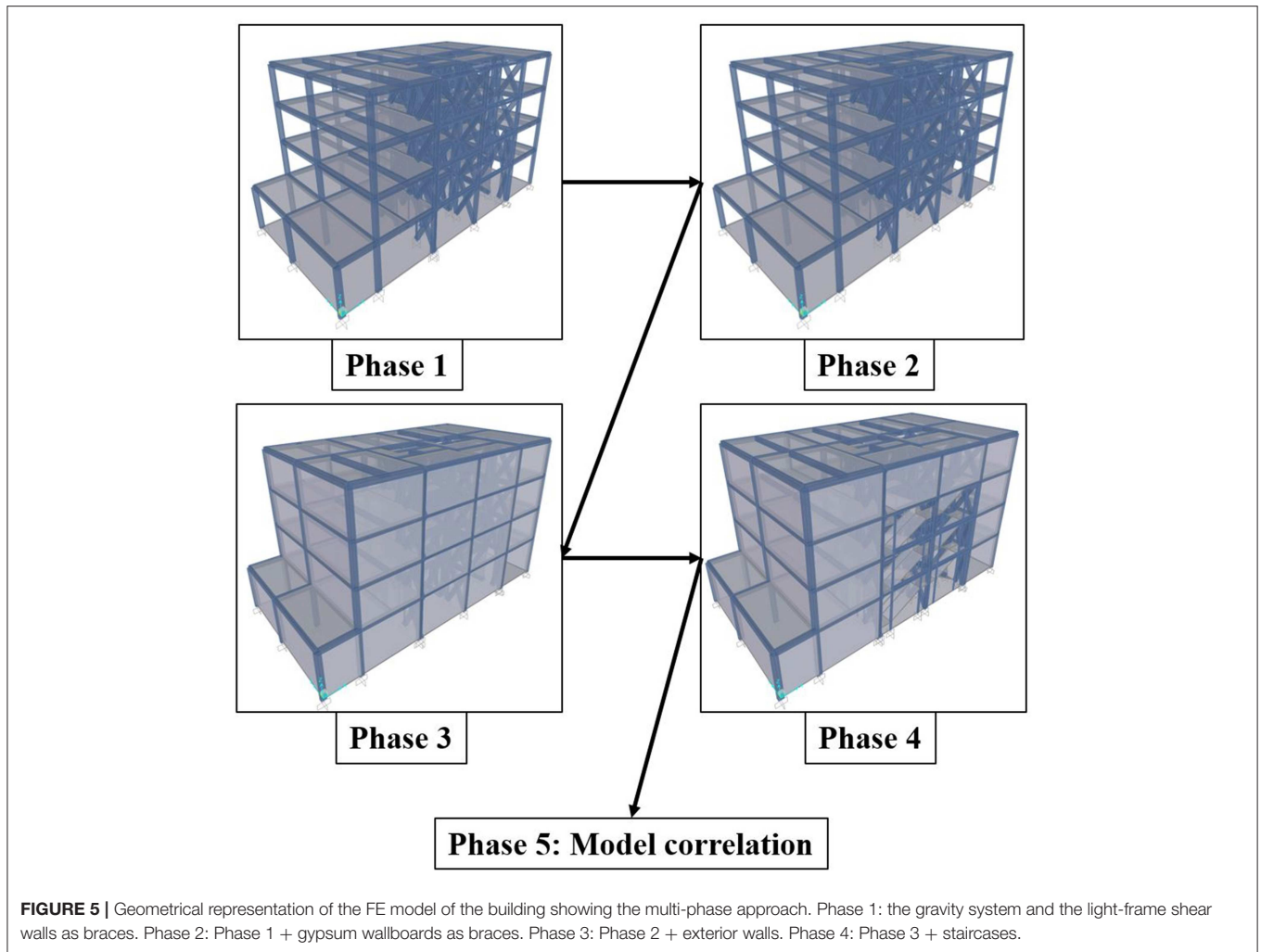
For the light-frame shear walls, the lateral stiffness of each shear wall section was modeled as two equivalent braces. The relation between the cross-brace stiffness and shear wall stiffness

is provided following recommendations from the Applied Technology Council (2017), which provides initial lateral stiffness values,  $K_0$ , for different configurations of light-frame shear walls, including those sheathed on two sides. A lateral stiffness,  $K_0$ , of 1,596 N/mm per meter (2,780 lb. per in. per ft.) was assigned, given the plywood shear wall size and detailing pattern.

All the wooden materials including the GLT beams and columns, CLT floors, and wood posts were assigned a density of 500 kg/m<sup>3</sup> (American Wood Council, 2015). To characterize the masses of the structure and the office supplies, masses were added at the floor and roof levels. The applied masses included the mass concrete screed (referred to as Gyp-Crete), carpet, office chairs and tables, books and roofing materials. **Table 3** summarizes the floor and roof added masses according to the building details and estimates of furniture observed in the office spaces.

Phase 2 of the modeling approach consisted of updating the light-frame shear walls stiffness to include the stiffness contribution of the gypsum wallboards (gwb) (Applied Technology Council, 2017). The same process used for the light-frame shear walls was applied to the gwb wall layers. The reported unit length lateral stiffness value amounts to 247 N/mm per m (430 lb./in. per ft.). Some wall sections displayed pairs of gwb layers on each side and therefore lateral stiffness of these walls was updated to reflect the number of gwb layers.

In the third modeling phase (Phase 3), the exterior walls were added to the model as isotropic shell elements. For the sheet metal façade, the lateral stiffness values of the shell elements were estimated by adding the stiffness of the sheet metal layer and the gwb layer to represent the sheet metal wall assembly. It was assumed that the sheet metal façade acts primarily through shear



behavior. Sheet metal in-plane shear modulus properties proved difficult to estimate from the construction details. Therefore, the shear modulus for the sheet metal was estimated from a previous study that evaluated the lateral stiffness of steel-clad wood framed (SCWF) walls (Aguilera, 2014). Aguilera (2014) evaluated the shear modulus and strength of SCWF wall assemblies typically seen in post-frame buildings. The study by Aguilera (2014) considered 17 SCWF shear walls of 4,880 mm (16') in width and 3,660 mm (12') in height, which were tested using a monotonic loading regime and with a cantilever wall setup. Seven different SCWF wall types were tested and differed in criteria such as shape of corrugation, girt spacing, fastener configurations. The mean shear modulus of all the SCWF shear walls tested was used to model the sheet metal façade stiffness and added to the exterior walls' gwb layer stiffness.

For the façade glazing, a lateral stiffness value of 410 N/mm per m (715 lb. per in. per ft.) of glass façade length was used. This stiffness value was estimated from glazing in-plane stiffness test conducted by Cruz et al. (2010) on a glass section of 1,200 mm (47.25") in height and 1,600 mm (63") in width, fastened to a

timber frame around its edges. The column-to-column distances were assigned as the width of the individual exterior wall shell elements and the story heights were assigned as the height of the exterior wall shell elements.

The stairs were added as isotropic shell elements for the landings, stairs threads and the stairs handrails. The stair landings and the handrails consist of 3-ply CLT panels, while the stairs threads consist of plywood material. The stiffness assigned to the CLT panels was derived using the Composite Theory Method (k-Method) as presented in the CLT Handbook (Gagnon and Popovski, 2011). The stair threads are made of plywood material with a thickness of 28.5 mm (1-1/8"). A modulus of elasticity (MOE) of 7,450 MPa (1,080 ksi) was assumed on the basis the MOE of Douglas-fir plywood sheathing products presented in the Wood Handbook (Forest Products Laboratory, 2010).

After the additions of the NSCs described in phase 2 through phase 4 were included to the model, a model correlation phase was added. The correlation phase was mainly added due to a disagreement observed between experimentally estimated and the model results for the torsional fundamental frequency. The correlation phase included reevaluating floor mass distributions

**TABLE 2** | Summary of stiffness properties.

Element	Phase	E (MPa)	$k_0$ (KN/mm/m)	G (MPa)
GLT beams and columns <sup>a</sup>	1	12,410	-	-
CLT floors <sup>a</sup>	1	12,410	-	-
Steel Hold-downs <sup>b</sup>	1	200,000	-	-
Light-frame shear walls (trusses) <sup>c</sup>	1	-	1,596	-
Gypsum board (trusses) <sup>c</sup>	2	-	247	-
Steel cladding <sup>d</sup>	3	-	-	155
Glazing <sup>e</sup>	3	-	-	114
Staircase landings and rails (CLT) <sup>f</sup>	4	11,700	-	-
Staircase threads (plywood) <sup>g</sup>	4	7,450	-	-

<sup>a</sup>American Wood Council (2015).

<sup>b</sup>American Institute of Steel Construction (2017).

<sup>c</sup>Applied Technology Council (2017).

<sup>d</sup>Aguilera (2014).

<sup>e</sup>Cruz et al. (2010).

<sup>f</sup>Gagnon and Popovski (2011).

<sup>g</sup>Forest Products Laboratory (2010).

and adjusting the stiffness contribution of the exterior sheet metal façade walls and the light-frame shear walls. The correlation phase is further discussed in section Parametric Study.

Lastly, a parametric study that included model parameter variations of structural and non-structural factors was conducted to examine the impact that several factors would have on the fundamental frequencies of the structure. The structural factors considered consisted of the global mass of the structure, the lateral stiffness of the light-frame shear walls, the lateral stiffness of the GLT members and the CLT diaphragm stiffness. Along with the structural factors, some non-structural factors were considered in parametric study, including the properties assigned to the sheet metal façade, window glazing, and staircases. A 25% deviation from the modeled values was applied to each of these factors. For the mass parameter, a unit area mass was added or subtracted to the total floor and roof areas.

## RESULTS

### Operational Modal Analysis: EFDD and SSI

Operational modal analysis (OMA) using EFDD resulted in the identification of several modal features of the vibration modes. **Figure 6A** shows the SVDs obtained using processing scheme 7 and Setup-1 and Setup-2 (**Table 1**). The plot shows the first three SVDs with the high-pass filter at 0.5 Hz and a decimation frequency of 20.48 Hz. Three well-defined peaks are discernable in the frequency range from 0–5 Hz for SVD1 to SVD3. For frequencies above 5 Hz, two peaks can be observed between 5–10 Hz.

**Figure 6B** shows the state space models stabilization plots for data processed using procedure 8 (**Table 1**). A maximum model order of 14 was selected (marked with a thick horizontal line) with the expectation that < 7 structural modes would be identified in the frequency range of 0 to 20.48 Hz. The vertical dots in the plot indicate the stable modes identified from data collected in Setup-2 only when using the processing scheme 8.

**TABLE 3** | Summary of mass estimates for floors and roof.

Item	Mass
Gyp-crete <sup>a</sup>	42.3
Sound barrier <sup>b</sup>	8.8
Carpet <sup>c</sup>	9.8
Office chairs, desk and books <sup>d</sup>	7.3
Floor Total (kg/m <sup>2</sup> )	68.2
Roofing material <sup>e</sup>	2.0
Insulation <sup>f</sup>	1.5
Mechanical units <sup>g</sup>	3.4
Roof Total (kg/m <sup>2</sup> )	6.9
Light-frame walls to floor (kg/m <sup>2</sup> ) <sup>a</sup>	176
Light-frame walls to roof (kg/m <sup>2</sup> ) <sup>a</sup>	88
Sheet metal façade to floor frame (kg/m) <sup>a</sup>	179
Sheet metal façade to roof frame (kg/m) <sup>a</sup>	89.5
Window glazing to floor frame (kg/m) <sup>h</sup>	89
Window glazing to roof frame (kg/m) <sup>h</sup>	44.5

<sup>a</sup>From Boise Cascade (2016) technical note on weights of building materials.

<sup>b</sup>From Homasote<sup>1</sup>

<sup>c</sup>Estimates based on local observation and engineering judgement.

<sup>d</sup>From Empire<sup>2</sup> West Title Agency web link.

<sup>e</sup>From GAF<sup>3</sup> web link.

<sup>f</sup>From Owens Corning<sup>4</sup> web link.

<sup>g</sup>From Daikin<sup>5</sup> web link.

<sup>h</sup>From Glass<sup>6</sup> Association of North America.

The modes are extracted in the frequency range of 0–5 Hz, two of which are closely spaced. One additional mode is extracted in the 5–10 Hz frequency range.

**Figure 7** summarizes the natural frequencies, damping ratios and the mode shapes identified using the EFDD and the SSI. The values in bold show the average natural frequencies and damping ratios resulting from all the processing schemes outlined in section Data Post-Processing and Analysis: Procedures and Methods. The values in parenthesis indicate minimum and maximum values of natural frequencies and damping ratios identified as a result from the different processing schemes. Four modes of vibrations were identified using both OMA methods. Three of these modes present the fundamental modes (NS lateral

<sup>1</sup>Homasote.com 440 Sound Barrier. Available at: <http://www.homasote.com/products/440-soundbarrier.com>

<sup>2</sup>Empire West Title Agency Average Weight of Common Household Furniture. ewtaz.com. Available at: <http://www.ewtaz.com/images/uploads/average-weight-furniture-2.pdf>

<sup>3</sup>GAF EverGuard TPO Membrane Data Sheet. Available at: [https://www.gaf.com/en-us/document-library/documents/commercialroofingsystems/everguardtpo/everguardtpo60membrane/everguard\\_tpo\\_60\\_mil\\_membrane\\_data\\_sheet.pdf](https://www.gaf.com/en-us/document-library/documents/commercialroofingsystems/everguardtpo/everguardtpo60membrane/everguard_tpo_60_mil_membrane_data_sheet.pdf)

<sup>4</sup>Owens Corning FOAMULAR Extruded Polystyrene. (XPS) Insulation Technical Bulletin. Available at: <https://dcpd6wotaa0mb.cloudfront.net/mdms/dms/EIS/10015702/10015702-ASTM-C578-Types-and-Physical-Properties-for-FOAMULAR-Tech.-Bulletin.pdf?v=1343093874000>

<sup>5</sup>Daikin Air Conditioning Technical Data. Available at: [http://www.daikintech.co.uk/Data/VRV-Outdoor/RXYQ/2014/RYYQ-T7Y1B/RYYQ-T7Y1B\\_Databook.pdf](http://www.daikintech.co.uk/Data/VRV-Outdoor/RXYQ/2014/RYYQ-T7Y1B/RYYQ-T7Y1B_Databook.pdf)

<sup>6</sup>Glass Association of North America Approximate Weight of Architectural Flat Glass. Available at: <http://www.syracuseglass.com/E-DOCS/general/EDOCS/Approximate%20Weight%20of%20Architectural%20Flat%20Glass.pdf>

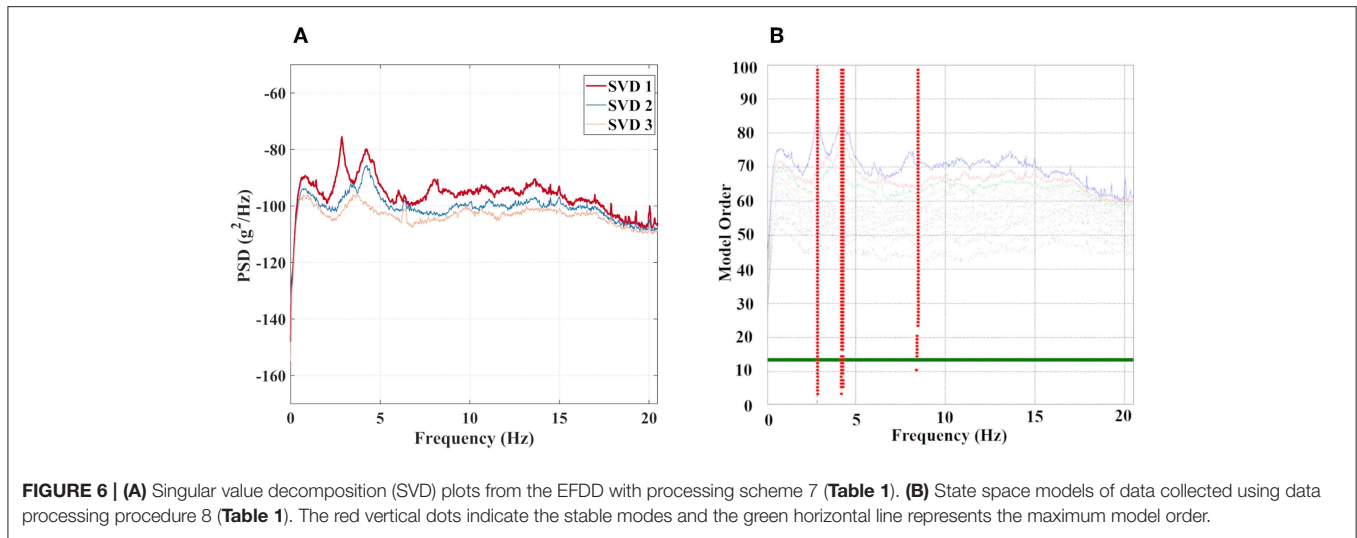


**FIGURE 6 | (A)** Singular value decomposition (SVD) plots from the EFDD with processing scheme 7 (Table 1). **(B)** State space models of data collected using data processing procedure 8 (Table 1). The red vertical dots indicate the stable modes and the green horizontal line represents the maximum model order.

1 <sup>st</sup> NS direction		1 <sup>st</sup> EW direction		1 <sup>st</sup> Torsional		2 <sup>nd</sup> NS direction	
EFDD	SSI	EFDD	SSI	EFDD	SSI	EFDD	SSI
$f$ (Hz) = <b>2.85</b> (2.84 – 2.86)	$f$ (Hz) = <b>2.86</b> (2.83 – 2.88)	$f$ (Hz) = <b>4.17</b> (4.12 – 4.23)	$f$ (Hz) = <b>4.20</b> (4.17 – 4.23)	$f$ (Hz) = <b>4.24</b> (4.23 – 4.25)	$f$ (Hz) = <b>4.29</b> (4.28 – 4.31)	$f$ (Hz) = <b>8.15</b> (8.10 – 8.19)	$f$ (Hz) = <b>8.27</b> (8.21 – 8.30)
$\zeta$ (%) = <b>2.40</b> (2.24 – 2.54)	$\zeta$ (%) = <b>3.13</b> (2.58 – 3.44)	$\zeta$ (%) = <b>1.29</b> (0.60 – 1.91)	$\zeta$ (%) = <b>4.09</b> (3.02 – 4.69)	$\zeta$ (%) = <b>1.38</b> (1.07 – 1.60)	$\zeta$ (%) = <b>5.66</b> (5.34 – 6.13)	$\zeta$ (%) = <b>4.66</b> (4.21 – 5.52)	$\zeta$ (%) = <b>7.76</b> (6.98 – 8.54)

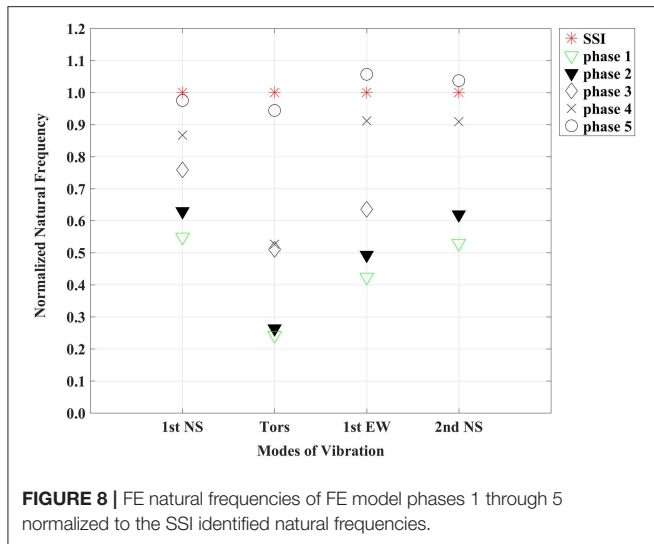
**FIGURE 7 |** OMA identified natural frequencies, damping ratios and mode shapes. The values in bold represent the mean natural frequencies and damping ratios from all the post-processing schemes. The parentheses indicate the minimum and maximum natural frequencies and damping ratios as a result of using the post-processing schemes as described in section Data Post-Processing and Analysis: Procedures and Methods.

direction, torsion, and EW lateral direction), and the fourth mode present the second mode in the NS direction of the building. There are slight variations in the average natural frequencies extracted from the two OMA methods. The largest natural frequency variation occurs in the second lateral NS direction mode amounting to 0.12 Hz (or 1.4% of the SSI extracted average natural frequency). These variations in natural frequencies are less significant than the damping ratios variations. For instance, the average fundamental EW mode’s damping ratio obtained by EFDD equated to 1.38% while the SSI obtained damping ratio for this mode was 5.66%. Several studies have explored damping ratios variations in closely spaced modes (Magalhães et al., 2010) and identifiability factors such as length of data

recorded, amplitude of excitation, spatial density of sensors, and measurement noise (Moaveni et al., 2014). The identified torsional and first EW direction modes are indeed closely spaced modes. This factor could help explain the large variations in damping ratios.

### Finite Element Model Results

Figure 8 shows the changes in the computed natural frequencies by adding phase 1 through phase 4 components in comparison with the SSI identified natural frequencies. The FE model natural frequencies are normalized to the respective SSI identified averaged natural frequencies. Figure 8 also shows effects of the correlation phase (phase 5) which will be discussed in section



Parametric Study. The natural frequencies computed from phase 1 were significantly lower than the natural frequencies of the ambient vibration testing. For instance, in the EW and NS directions. They corresponded to 41 and 55% of the natural frequencies obtained through SSI. The first torsional natural frequency amounted 25% of the torsional natural frequency obtained by SSI. After the addition of the gwb layers of the shear walls (phase 2), the fundamental frequencies increased to 48 and 63% in the EW and NS directions, respectively. The first torsional natural frequency, however, was marginally increased in phase 2, reaching 27% of the experimental torsional natural frequency. The large difference in the torsional fundamental frequency in phase 1 and phase 2 is consistent with the concept that the light-frame shear walls, that are located around the center and south-to-center of the building, would contribute less torsional stiffness to the overall structural system.

After the addition of the sheet metal façade and the window glazing in phase 3, the fundamental natural frequency in the NS direction increased to 76% of the ambient testing fundamental frequency. A significant increase was observed in the FE torsional fundamental frequency, going up to 52% of the SSI identified torsional natural frequency. This observation confirms that the exterior non-structural walls contribute significantly to the torsion stiffness of the building.

Phase 4, which featured the addition of the staircases, increased of the EW and NS fundamental frequencies to 91 and 87%, respectively. The addition of the staircases resulted in the FE model torsional fundamental frequency adding up to 53% of the SSI identified natural frequency.

The mode shapes features resulting from the two OMA methods and the FE model were compared for consistency using the Modal Assurance Criterion (Pastor et al., 2012). The Modal Assurance Criterion (MAC) is given by:

$$\text{MAC}(\phi_i, \phi_j) = \frac{|\phi_i^T \phi_j|^2}{(\phi_i^T \phi_i)(\phi_j^T \phi_j)} \quad (1)$$

where  $\phi_i$  is the modal vector at frequency  $i$  and  $\phi_j$  is the modal vector at frequency  $j$ .

The diagonal MAC values resulting from the OMA methods and the FE model are presented in **Figure 9A**. The diagonal MAC values between the EFDD and SSI identified modal vectors show high levels of consistency (above 0.9), except for the first EW direction mode which show a significantly low MAC value. To further investigate the possible reasons for the low MAC value in the fundamental EW mode, shorter segments of collected data were analyzed for MAC consistency. The lack of consistency in terms of MAC values on subsets of collected data could indicate some limitations in identifiability. Two 5-min segments collected data were analyzed separately, from setup 1 and from setup 2. The fundamental EW direction MAC value becomes 0.69 when the 5-min setup 1-only data is used as shown in **Figure 9B**. The EW direction mode is not identifiable using the setup 2-only 5-min segment. When data for the two (2) 5-min segments are combined, the MAC value becomes 0.74. Yet when the full data set is considered, the EW direction MAC value is 0.12. While the fundamental EW direction MAC value is higher when considering certain portions of the data, the entire data set yields a lower MAC value. This points to the limitations in consistently extracting the EW mode shape using both OMA methods, which is likely due to the EW mode's proximity to the torsional mode.

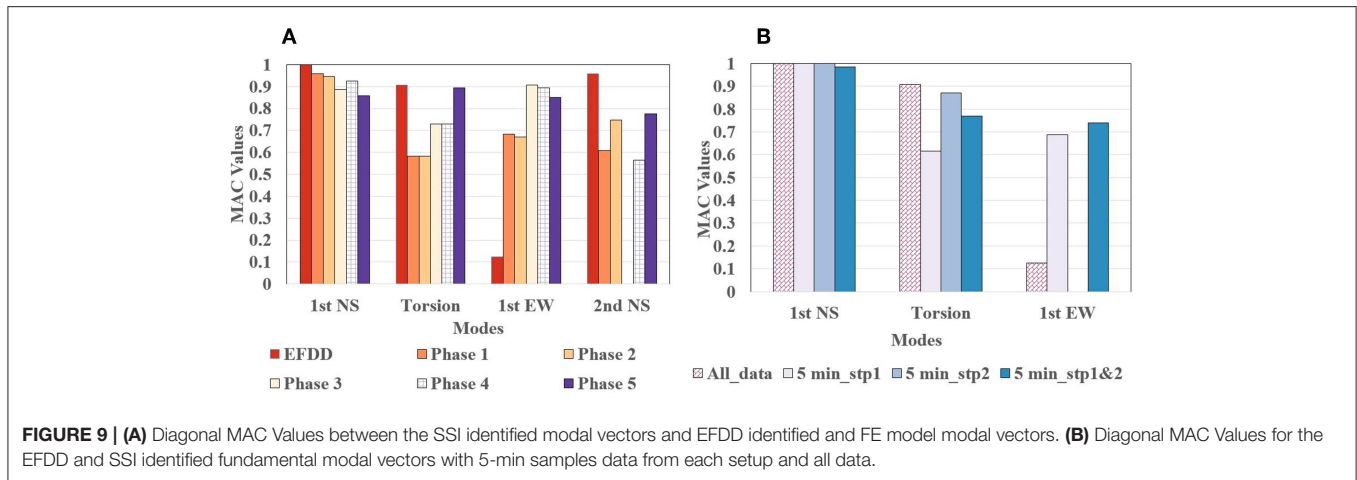
The diagonal MAC values of the FE model modes and SSI identified modes show an increasing trend for torsional and EW direction fundamental modes as the additional model components are added (see **Figure 9A**). The NS direction MAC value decreases as additional stiffness members are added and equates to 0.92 after phase 4.

## Model Correlation

While the modeled lateral natural frequencies were converging toward the SSI identified natural frequencies after phase 4, the torsional natural frequency amounted only to 53% of the identified torsional fundamental frequency. Phase 5 was introduced to correlate the FE model torsional fundamental frequency to the experimentally identified values. The difference in torsional natural frequencies between the FE model and the SSI method could be attributed to two factors: a mischaracterization of floor mass distribution and/or a difference in the lateral stiffness contribution of structural and non-structural building components.

The masses of the building components were estimated by considering the main members without the masses of their connecting assemblies. This would suggest that the building's total mass is underestimated, given that most of the member connections are made of steel, a significantly denser material compared to wood, and that real moisture condition weights are expected to be larger than the nominal values assumed per NDS. The locations where the underestimations of masses could most likely be higher are the exterior walls. The masses that were not estimated would include the steel furring and connections of the façade to the structural system, and the window glazing framing.

The second factor that plays into the imbalance observed in the torsional natural frequency can be attributed to the stiffness distribution along the horizontal planes. The torsional stiffness



is proportional to the square of the eccentricity between the axis of stiffness and the center of mass. For this reason, the stiffness distribution could play an important role adjusting the torsional stiffness and consequently the torsional frequency. For the Albina Yard, the stiffness distribution was evaluated by adjusting the stiffness values of the light-frame shear walls and non-structural lateral stiffness contributors as specified in phase 1 through phase 4. The modeled exterior walls stiffness most likely present sources of biases due to the fact that they were selected from other experimental walls that may vary considerably from the structure's exterior wall stiffness values. In the case of the sheet metal façade, shear modulus is the factor of both the warping action and slipping in connections in addition to the thickness of the metal profile. As result of these factors, sheet metal shear modulus can be orders of magnitude lower than continuous profiles of similar thickness as stated by Luttrell (2004). Due to the lack of connection details on the exterior walls, it was determined to adjust stiffness with the goal of matching the torsional natural frequency while maintaining the lateral natural frequencies close to their original values. The stiffness distribution adjustment entailed increasing the stiffness of some lateral resisting components, while decreasing the stiffness of to maintain the balance in natural frequencies in the two orthogonal directions and in-plane torsion. It was observed that an increase in the exterior walls' stiffness coupled with a reduction in the stiffness of staircases and light-frame shear walls was leading to an increase in the torsional natural frequency while maintaining the lateral natural frequencies relatively similar to the experimental values.

The two calibration approaches involved the addition of masses to the exterior walls and the increase in exterior walls stiffness coupled with the reduction of other stiffness contributors. The combination of these two approaches led to the natural frequencies converging for both the lateral and torsional modes. The resulting FE natural frequencies are 2.79 Hz in the NS direction, 4.05 Hz in the torsional direction and 4.44 Hz in the EW direction. These natural frequencies are a result of increasing the exterior walls (glazing and metal façade) masses by a factor of two (2). The stiffness of the metal façade and the glazing were

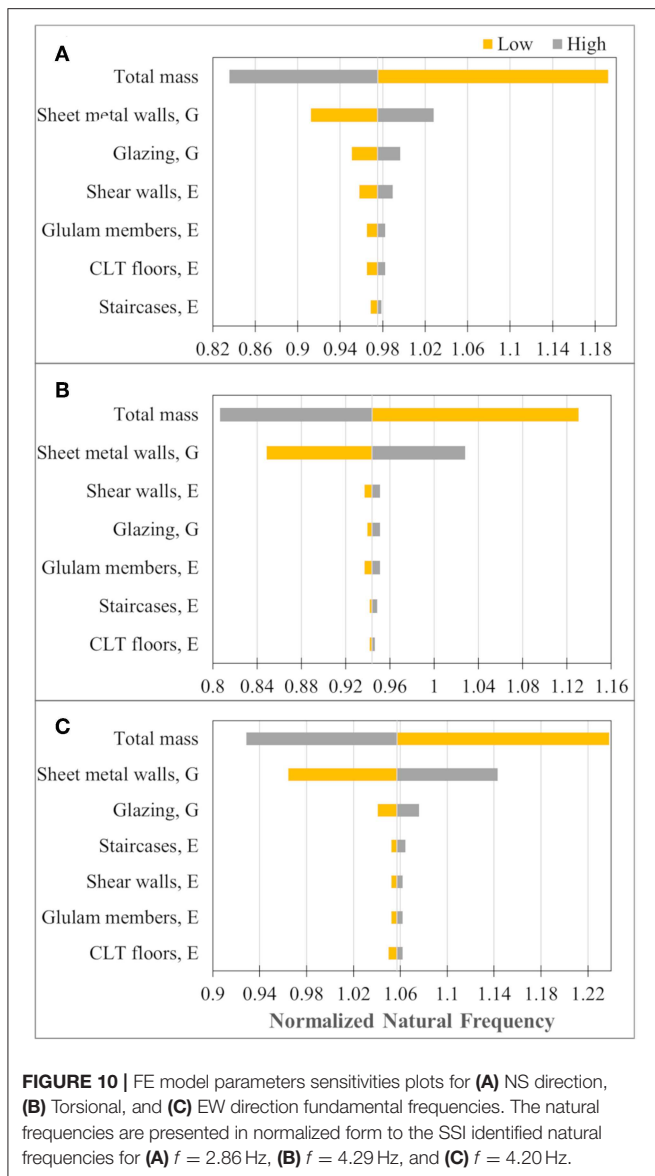
multiplied by factors of 10.25 ( $G = 1,586$  MPa) and 2.8 ( $G = 320$  MPa) of the respective initially modeled values. The increase in the stiffness of the exterior walls was coupled with light-frame shear walls and the staircases stiffness values reduced by a factor of two (2) and four (4), respectively.

## Parametric Study

The parametric study considered the effects a 25% change in the parameters described in section Structural Modeling to the fundamental frequencies of the FE model. **Figure 10** presents the results of the parametric studies on the NS direction, torsional, and EW direction fundamental frequencies. The results in this figure are normalized to the respective fundamental frequency identified through the SSI method. **Figure 10A** shows that the total mass exerts the most influence on the NS fundamental frequency, followed by the sheet metal façade. The total mass of the structure has the most influence on the natural frequencies in comparison to the stiffness parameters since it is one of the two factors in fundamental frequency equation,  $f = 2\pi\sqrt{\frac{k}{m}}$ . The stiffness parameters considered in this parametric study contribute to the system total lateral stiffness,  $k$ . Inherently, the mass has larger effect on the change in natural frequency compared to the single stiffness parameters.

The window glazing, light-frame shear walls, GLT members, CLT floors stiffness influence the NS direction fundamental frequency to a lower degree compared to the total mass and the sheet metal façade stiffness. The light-frame shear walls contribute less to the NS direction fundamental frequency than the sheet metal façade and the window glazing, which are considered to be non-structural building components.

**Figure 10B** shows the effects of the seven considered parameters to the torsional fundamental frequency. Similar to the case of the fundamental frequency in the NS direction, the total mass of the building displays the most influence on the torsional fundamental frequency. The sheet metal façade stiffness, although often considered as a non-structural building component, causes more effect to the torsional fundamental frequency than the light-frame shear walls stiffness. The window



glazing, the light-frame shear walls and the glulam members' stiffness have a lower impact to the torsional fundamental frequency compared to the mass and the sheet metal façade stiffness. The torsional natural frequency is least affected by the change in parameters of the staircases and CLT floors stiffness.

**Figure 10C** shows the effects of the parameters to the EW direction fundamental frequency. The total mass shows to be the most contributing factor as observed for the two other fundamental frequency cases. The sheet metal façade stiffness has a noticeable effect on the fundamental frequency in the EW direction, and exerts more influence than the light-frame shear walls. For the EW direction, the exterior walls have more impact to the fundamental frequency than the staircases, light-frame shear walls, GLT members, and CLT floors.

Among the structural and non-structural stiffness parameters, the sheet metal façade and the glazing exert the most influence

in the fundamental frequencies. Based on this observation, it can be suggested that at the ambient level of excitations, the exterior walls have the most impact in the structure's response to ambient excitations. As expected, the fundamental frequencies are much less sensitive to the change of the CLT floors in-plane stiffness compared to the other stiffness parameters considered. While it is expected that the in-plane shear modulus of CLT is smaller compared to the modulus of elasticity considered in this study, based on this sensitivity study, the in-plane shear modulus stiffness is not expected to have a major impact on the fundamental frequencies.

## DISCUSSION

### Comparison Between EFDD and SSI

Four modes were identified with both of the OMA methods and provide confidence in the results. The identified modes compared to each other well in terms of natural frequency (see **Figure 7**) and mode shapes (**Figure 8A**). The closely-spaced modes provided challenges in modal identifiability. While the OMA methods were consistent in extracting the natural frequencies of the closely spaced modes, their mode shapes proved difficult to differentiate. By analyzing two 5-min segments of recorded data from setup 1 and 2, the diagonal MAC value between the EFDD and SSI identified closely spaced modes varied significantly, while the MAC value for NS direction fundamental frequency was consistently high regardless of recorded data length and changes in sensor locations. Possible causes for the lack of consistency in the EW direction mode shapes can be due primarily to its proximity to the torsional mode but also to other identifiability factors such as the presence of measurements noise, and the limited number of sensor locations.

In contrast to the small difference in natural frequency values observed across setups and methods, a large difference was observed in the extracted damping ratios. However, such differences are to be expected and have been discussed in other studies (e.g., Magalhães et al., 2010; Moaveni et al., 2014; Yu et al., 2017). This is most likely due to larger estimation variance and bias for damping ratios compared to natural frequencies (Pintelon et al., 2007; Reynders et al., 2008).

### Comparison Between FE Model and Dynamic Testing Identification Results

After model calibration, the model natural frequencies showed to match the experimental natural frequencies in the three fundamental modes (NS lateral, EW lateral, torsional directions) and one higher mode (second NS lateral).

The calibrated FE model suggests that non-structural building components play a significant role in the measured ambient vibration excitations. When comparing fundamental frequencies in the NS direction between phase 1 and phase 5 (see **Figure 8**), an increase from 1.57 to 2.79 Hz is observed. This increase in fundamental frequency, as a result of the non-structural components, shows a similar trend to the increases observed by Folz and Filiatrault (2004b) in a laboratory setting, where the fundamental frequency increased from 3.28 to 6.95 Hz after the addition of non-structural components.

The correlation phase results also suggest that, at ambient levels of excitation, the exterior walls stiffness contributes more to the lateral and torsional natural frequencies than the stiffness of the light-frame shear walls, the interior gravity frames and the staircases. The parametric study, conducted to investigate the effects of different structural and non-structural parameters to the three fundamental natural frequencies, showed that the overall mass of the building has the most influence on the fundamental frequencies. For a 25% reduction in the total building mass, the model normalized torsional fundamental frequency increased from a ratio of 0.96 to 1.15 of the torsional fundamental frequency identified with the SSI method (see **Figure 10B**). This change is equivalent to a 20% natural frequency increase in relation to the torsional natural frequency of the correlated FE model. In the NS and EW directions, the 25% decrease in total mass resulted in a 21 and 17% increase in the fundamental frequencies, respectively. This finding support, for FE modeling, the importance of the estimation the structure's dead loads and weights, as well as of a good approximation of the masses acting on the building at the time of the experimental testing. Experimental studies such as Assi et al. (2016) observed a similar effect with as much as a 21.7% reduction in the identified natural frequency after the addition of some non-structural components to a six-story building featuring a reinforced concrete shear walls and moment resisting frames as lateral resisting structural system. It is also worth noting that more accurate estimation of the wood specific gravity could be done by adjusting the reference values, such as those provided by NDS (American Wood Council, 2015), to actual moisture content data measured at the site.

The parametric phase also indicated that the exterior sheet metal walls exerts the most influence among all the lateral stiffness contributors including the light-frame shear walls. Most often, researchers and design practitioners have a limited amount of information on the structural properties of façade elements. Thus, structural modeling often excludes the stiffness addition of non-structural components. The FE modeling results points to the potential benefits of including the stiffness of non-structural components to improve the understanding of dynamic behavior of tall mass timber structures under service lateral loads such as wind loads.

### Comparison of Identified Fundamental Frequencies to Code Approximate Fundamental Frequency Equation

ASCE 7-16 (American Society of Civil Engineers, 2017) provides guidelines for estimating the fundamental period of a building based on its height or the number of stories. The approximate fundamental period calculation is used as a part of the Equivalent Lateral Force (ELF) procedure, a common procedure for analyzing seismic loads on structures. The fundamental frequencies in the lateral directions as well as the torsional fundamental frequency from the ambient vibration results are compared to the fundamental frequencies derived from the fundamental period equation:

$$T_a = C_t h_n^x \quad (2)$$

where  $C_t$  and  $h_n^x$  are parameters that correspond to 0.048 and 0.75 for light-frame structures. The resulting approximate fundamental period is equal to 0.38 s and corresponds to a natural frequency of 2.63 Hz. By comparison, the approximate fundamental frequency is a close approximation to the identified fundamental frequency in the NS direction. In the EW direction and torsion, Equation (6) does not provide a good estimate of the measured frequencies. It is worth noting, however, that under seismic loading, the stiffness contribution of the non-structural elements is expected to be smaller.

## CONCLUSION AND RECOMMENDATIONS

An ambient vibration test was conducted on a four-story mass timber, commercial building. This experimental study provides a unique benchmark dataset on the first construction using CLT produced in the U.S. Two OMA methods were used to identify natural frequencies, damping ratios, and mode shapes of the building. Four structural modes were identified and compared to those obtained using a correlated model that was developed using a phased finite element model updating approach. The four structural modes identified are the first three fundamental structural modes (EW, NS and torsional directions) and one higher lateral structural mode (NS direction). Reasons causing limitation in identifiability of the higher modes include use of an insufficient number of sensors, non-ideal sensor locations, presence of closely spaced structural modes, and limited level of the energy of excitation. It is well-known that these factors can increase bias and variance of the modal identification.

The presence of mechanical sources of excitation that are commonly found in buildings that are under operation can further interfere with the determination of modal properties. The use of different types of accelerometers led to additional identifiability limitations due to issues such as scaling and sensor sensitivity. Despite the variability in modal parameters arising from each method, use of both OMA methods was useful in improving confidence in the results.

A parametric study assessing the contribution of seven structural and non-structural factors to the fundamental frequencies was conducted. The mass of the building was identified as the factor that most affected all three fundamental frequencies. Therefore, a careful estimation of the building masses and its distribution in plan is crucial for accurate dynamic modeling of ambient responses. While the stiffness of non-structural members is often not considered for high amplitude level of lateral excitations, such as extreme seismic or wind loading conditions, the correlation between the identified modal features and the FE model highlights that exterior non-structural walls play a major role in the responses to ambient excitations, which is important when assessing serviceability and comfort of the occupants. The effects of non-structural members to the lateral response of tall mass-timber structures will need to be further investigated as new heights of timber buildings are reached and serviceability limit states may govern design.

## AUTHOR CONTRIBUTIONS

AB and MR conceived the study. AB and IM performed the experimental design. IM, AB, and MR carried out the *in-situ* data collection. IM performed the data processing and finite element modeling with guidance from AB and MR. IM took the lead on drafting the article with critical input from AB and MR through the writing process. AB and MR contributed to the interpretation of results and carried out the editing process.

## FUNDING

Funding for this study was provided by the U.S. Department of Agriculture Agricultural Research Service (USDA ARS) Agreement No. 58-0202-5-001 through the TallWood Design Institute at Oregon State University. This study was also funded

## REFERENCES

- Aguilera, D. (2014). *Development of strength and stiffness design values for steel-clad, wood-framed diaphragms* (Master thesis). Washington State University, Pullman, WA.
- American Institute of Steel Construction (2017). *Steel Construction Manual, 15th Edn.* Chicago, IL: AISC.
- American National Standards Institute/APA—The Engineered Wood Association (2018). *Standard for Performance-Rated Cross Laminated Timber*. Tacoma, WA: ANSI/APA PRG-320.
- American Society of Civil Engineers (2017). *Minimum Design Loads and Associated Criteria for Buildings and Other Structures*. Reston, VA: American Society of Civil Engineers
- American Wood Council (2015). *National Design Specification (NDS) Supplement: Design Values for Wood Construction 2015 Edition*. Leesburg, VA: American Wood Council.
- Applied Technology Council (2017). *Recommended Modeling Parameters and Acceptance Criteria for Nonlinear Analysis in Support of Seismic Evaluation, Retrofit, and Design*. Gaithersburg, MD: Applied Technology Council.
- ARTEMIS Modal (2017). Available online at: [http://www.svibs.com/products/ARTEMIS\\_Modal.aspx](http://www.svibs.com/products/ARTEMIS_Modal.aspx) (accessed April 15, 2018).
- Asgarian, A., and McClure, G. (2012). "Impact of seismic retrofit and presence of terra cotta masonry walls on the dynamic properties of a hospital building in Montréal, Canada," in *15th World Conference on Earthquake Engineering* (Lisbon).
- Assi, R., Youance, S., Bonne, A., and Nollet, M.-J. (2016). "Effect of non-structural components on the modal properties of buildings using ambient vibration testing," in *CSCE Resilient Infrastructure* (London).
- Boise Cascade (2016). *Weights of Building Materials*, 1–2. Available online at: [https://p.widencdn.net/yws0s3/GE-1\\_Weights\\_Building\\_Materials](https://p.widencdn.net/yws0s3/GE-1_Weights_Building_Materials) (accessed June 26, 2019).
- Brincker, R., and Andersen, P. (2006). "Understanding stochastic subspace identification," in *Proceedings of the 24th International Modal Analysis Conference* (St. Louis, MO), 461–466.
- Brincker, R., Zhang, L., and Andersen, P. (2001). Modal identification of output-only systems using frequency domain decomposition. *Smart Mater. Struct.* 10, 441–445. doi: 10.1088/0964-1726/10/3/303
- Camelo, V., Beck, J., and Hall, J. (2002). *Dynamic Characteristics of Woodframe Structures*. Richmond, CA: Consortium of Universities for Research in Earthquake Engineering (CUREE) - Caltech Woodframe Project.
- Chopra, A. K. (2012). "Natural vibration frequency by rayleigh's method," in *Dynamics of Structures* (Pearson), ed William J. Hall, 330–334.
- Çelebi, M., Phan, L. T., and Marshall, R. D. (1993). Dynamic characteristics of five tall buildings during strong and low-amplitude motions. *Struct. Des. Tall Build.* 2, 1–15. doi: 10.1002/tal.4320020102

by the McIntire Stennis project (contract number 1009740) provided by the National Institute of Food and Agriculture, U.S. Department of Agriculture. The first author received a Graduate Teaching Assistantship from the Civil Engineering Department of Oregon State University during the year in which data collection was conducted.

## ACKNOWLEDGMENTS

The authors would like to acknowledge the individuals who helped with the data collection namely Rajendra Soti, Leonardo Rodrigues, James Batti, and Evan Schmidt; others who provided valuable technical guidance include Reid Zimmerman, Eric McDonnell, and Palle Andersen. Authors would like to thank the building owner, reworks Inc., and Lever Architecture for providing access to the building.

- Clinton, J. F., Bradford, S. C., Heaton, T. H., and Favela, J. (2006). The observed wander of the natural frequencies in a structure. *Bull. Seismol. Soc. Am.* 96, 237–257. doi: 10.1785/0120050052
- Collins, M., Kasal, B., Paevere, P., and Foliente, G. C. (2005a). Three-dimensional model of light frame wood buildings. i: model description. *J. Struct. Eng.* 131, 676–683. doi: 10.1061/(ASCE)0733-9445(2005)131:4(676)
- Collins, M., Kasal, B., Paevere, P., and Foliente, G. C. (2005b). Three-dimensional model of light frame wood buildings. II: experimental investigation and validation of analytical model. *J. Struct. Eng.* 131, 684–692. doi: 10.1061/(ASCE)0733-9445(2005)131:4(684)
- Cruz, P. J. S., Pequeno, J., Lebet, J.-P., and Mocibob, D. (2010). "Mechanical modelling of in-plane loaded glass panes," in *Challenging Glass 2 - Conference on Architectural and Structural Applications of Glass* (Delft).
- CSI (Computers and Structures, Inc). (2017). *SAP2000: Integrated Software for Structural Analysis and Design, Ver. 19*. Berkeley, CA: CSI.
- Devin, A., and Fanning, P. (2012). The evolving dynamic response of a four storey reinforced concrete structure during construction. *Shock Vib.* 19, 1051–1059. doi: 10.1155/2012/260926
- Ellis, B. R., and Bougard, A. J. (2001). Dynamic testing and stiffness evaluation of a six-storey timber framed building during construction. *Eng. Struct.* 23, 1232–1242. doi: 10.1016/S0141-0296(01)00033-5
- Folz, B., and Filiatrault, A. (2004a). Seismic analysis of woodframe structures. i: model formulation. *J. Struct. Eng.* 130, 1353–1360. doi: 10.1061/(ASCE)0733-9445(2004)130:9(1353)
- Folz, B., and Filiatrault, A. (2004b). Seismic analysis of woodframe structures. ii: model implementation and verification. *J. Struct. Eng.* 130, 1361–1370. doi: 10.1061/(ASCE)0733-9445(2004)130:9(1361)
- Forest Products Laboratory (2010). *(U.S.) Wood Handbook: Wood as an Engineering Material*. Madison, WI: Forest Products Laboratory.
- Freres, T. (2018). *Wood Panel Assemblies and Methods of Production*. Available online at: <https://patents.google.com/patent/US20180250920A1/en> (accessed February 02, 2018).
- Gagnon, S., and Popovski, M. (2011). "Structural design of cross-laminated timber elements," in *CLT Handbook: Cross-Laminated Timber - Canada Edition*, eds S. Gagnon and C. Pirvu (Pointe-Claire, QC: FPInnovations), 12–14.
- Gres, S., Andersen, P., Hoen, C., and Damkilde, L. (2019). "Orthogonal projection-based harmonic signal removal for operational modal analysis," in *Structural Health Monitoring, Photogrammetry and DIC, Volume 6. Conference Proceedings of the Society for Experimental Mechanics Series*, eds C. Niezrecki and J. Baqersad (Cham: Springer).
- Hafeez, G., Doudak, G., and McClure, G. (2018). Establishing the fundamental period of light-frame wood buildings on the basis of ambient vibration tests. *Can. J. Civ. Eng.* 45, 752–765. doi: 10.1139/cjce-2017-0348
- Hu, L., Karsh, E., Gagnon, S., Dagenais, C., and Ramzi, R. (2016). "Dynamic performance measured on two 6-storey buildings made from wood structures

- before and after their completion and occupancy,” in *Proceedings of the WCTE 2016 World Conference on Timber Engineering* (Vienna).
- Ivanović, S., Trifunac, M., Novikova, E., Gladkov, A., and Todorovska, M. (2000). Ambient vibration tests of a seven-story reinforced concrete building in Van Nuys, California, damaged by the 1994 Northridge earthquake. *Soil Dyn. Earthq. Eng.* 19, 391–411. doi: 10.1016/S0267-7261(00)00025-7
- Kharrazi, M. H. K., and Ventura, C. E. (2006). Vibration frequencies of woodframe residential construction. *Earthq. Spectra* 22, 1015–1034. doi: 10.1193/1.2360699
- Li, B., Hutchinson, G. L., and Duffield, C. F. (2011). The influence of non-structural components on tall building stiffness. *Struct. Des. Tall Spec. Build.* 20, 853–870. doi: 10.1002/tal.565
- Luttrell, L. D. (2004). *Steel Deck Institute Diaphragm Design Manual. Third Edition.* Fox River Grove, IL.
- Magalhães, F., Brincker, R., Cunha, Á., Caetano, E., and Brincker, R. (2007). “Damping estimation using free decays and ambient vibration tests,” in *Proceedings of the 2nd International Operational Modal Analysis Conference* (Copenhagen), 513–521.
- Magalhães, F., Cunha, Á., Caetano, E., and Brincker, R. (2010). Damping estimation using free decays and ambient vibration tests. *Mech. Syst. Signal Process.* 24, 1274–1290. doi: 10.1016/j.ymssp.2009.02.011
- Michel, C., Guéguen, P., El Arem, S., Mazars, J., and Kotronis, P. (2009). Full-scale dynamic response of an RC building under weak seismic motions using earthquake recordings, ambient vibrations and modelling. *Earthq. Eng. Struct. Dyn.* 39, 419–441. doi: 10.1002/eqe.948
- Moaveni, B., Barbosa, A. R., Conte, J. P., and Hemez, F. M. (2014). Uncertainty analysis of system identification results obtained for a seven-story building slice tested on the UCSD-NEES shake table. *Struct. Control Heal. Monit.* 21, 466–483. doi: 10.1002/stc.1577
- Mugabo, I., Barbosa, A. R., Riggio, M., and Batti, J. (2019). Ambient vibration measurement data of a four-story mass timber building. *Front. Built Environ.* 5:67. doi: 10.3389/fbuil.2019.00067
- Nayeri, R. D., Masri, S. F., Ghanem, R. G., and Nigbor, R. L. (2008). A novel approach for the structural identification and monitoring of a full-scale 17-story building based on ambient vibration measurements. *Smart Mater. Struct.* 17:025006. doi: 10.1088/0964-1726/17/2/025006
- Nguyen, T. T., Dao, T. N., Aaleti, S., van de Lindt, J. W., and Fridley, K. J. (2018). Seismic assessment of a three-story wood building with an integrated CLT-lightframe system using RTHS. *Eng. Struct.* 167, 695–704. doi: 10.1016/j.engstruct.2018.01.025
- Pastor, M., Binda, M., and Harčarik, T. (2012). Modal assurance criterion. *Procedia Eng.* 48, 543–548. doi: 10.1016/j.proeng.2012.09.551
- Pei, S., Rammer, D., Popovski, M., Williamson, T., Line, P., Lindt, J. W., et al. (2016). “An overview of CLT research and implementation in North America,” in *Proceedings of the WCTE 2016 World Conference on Timber Engineering* (Vienna).
- Pintelon, R., Guillaume, P., and Schoukens, J. (2007). Uncertainty calculation in (operational) modal analysis. *Mech. Syst. Signal Process.* 21, 2359–2373. doi: 10.1016/j.ymssp.2006.11.007
- Reynders, E., Pintelon, R., and De Roeck, G. (2008). Uncertainty bounds on modal parameters obtained from stochastic subspace identification. *Mech. Syst. Signal Process.* 22, 948–969. doi: 10.1016/j.ymssp.2007.10.009
- Reynolds, T., Bolmsvik, Å., Vessby, J., Chang, W., Harris, R., Bawcombe, J., et al. (2014). “Ambient vibration testing and modal analysis of multi-storey cross-laminated timber buildings multi-storey cross-laminated timber buildings,” in *World Conference on Timber Engineering* (Quebec city).
- Reynolds, T., Casagrande, D., and Tomasi, R. (2016). Comparison of multi-storey cross-laminated timber and timber frame buildings by in situ modal analysis. *Constr. Build. Mater.* 102, 1009–1017. doi: 10.1016/j.conbuildmat.2015.09.056
- Reynolds, T., Harris, R., Chang, W.-S., Bregulla, J., and Bawcombe, J. (2015). Ambient vibration tests of a cross-laminated timber building. *Proc. Inst. Civ. Eng. Constr. Mater.* 168, 121–131. doi: 10.1680/coma.14.00047
- Satake, N., Suda, K., Arakawa, T., Sasaki, A., and Tamura, Y. (2003). Damping evaluation using full-scale data of buildings in Japan. *J. Struct. Eng.* 129, 470–477. doi: 10.1061/(ASCE)0733-9445(2003)129:4(470)
- Soyoz, S., Taciroglu, E., Orakcal, K., Nigbor, R., Skolnik, D., Lus, H., et al. (2013). Ambient and forced vibration testing of a reinforced concrete building before and after its seismic retrofitting. *J. Struct. Eng.* 139, 1741–1752. doi: 10.1061/(ASCE)ST.1943-541X.0000568
- Steiger, R., Feltrin, G., Weber, F., Nerbano, S., and Motavalli, M. (2016). “On-site dynamic testing of a light-frame timber building,” in *Proceedings of the WCTE 2016 World Conference on Timber Engineering* (Vienna).
- Tarabia, A. M., and Itani, R. Y. (1997). Seismic response of light-frame wood buildings. *J. Struct. Eng.* 123, 1470–1477. doi: 10.1061/(ASCE)0733-9445(1997)123:11(1470)
- Yu, H., Mohammed, M. A., Mohammadi, M. E., Moaveni, B., Barbosa, A. R., Stavridis, A., et al. (2017). Structural Identification of an 18-story RC building in Nepal using post-earthquake ambient vibration and lidar data. *Front. Built Environ.* 3:11. doi: 10.3389/fbuil.2017.00011

**Conflict of Interest Statement:** The authors declare that the research was conducted in the absence of any commercial or financial relationships that could be construed as a potential conflict of interest.

Copyright © 2019 Mugabo, Barbosa and Riggio. This is an open-access article distributed under the terms of the Creative Commons Attribution License (CC BY). The use, distribution or reproduction in other forums is permitted, provided the original author(s) and the copyright owner(s) are credited and that the original publication in this journal is cited, in accordance with accepted academic practice. No use, distribution or reproduction is permitted which does not comply with these terms.